POPULAR SUMMARY

**Westerly Wind Events in the Eastern Indian Ocean as a Precursor to El Niño: A Case Study for the 2002-03 El Niño**

Scott Curtis, Robert F. Adler, George J. Huffman, and Guojun Gu
Submitted Journal of Climate

This paper extends the work of our previous study, which showed the potential of using precipitation in the eastern Indian Ocean to predict when an El Niño would begin. The paper begins by showing the successful prediction of the 2002-03 El Niño. However, precipitation is really used as a substitute for wind (storms are usually accompanied by heavy wind), because a popular hypothesis is that winds (especially winds out of the West) stir up the ocean surface in the western Pacific sending currents of warm waters to the east Pacific where El Niños form. This paper shows that it is typical for storms that produce strong winds in the western Pacific to have traveled from the Indian Ocean. We begin in the Indian Ocean looking at strong bursts of wind over several days. The number of windy days seems to increase in the months prior to El Niño. We examined these relationships in detail for November 2001 to April 2002, before the recent El Niño, using NASA's TRMM and QuikSCAT data. We found in one case that a warming of the eastern Indian Ocean occurred about 25 days before heavy rainfall formed. As the stormed moved eastward it was followed (6 days later) by strong winds out of the West. The entire storm system (and warming of the sea) moved eastward through a small strip of water between Indonesia and Australia, before reaching the western Pacific. Thus, this paper increases our understanding of the physical processes leading to the formation of El Niño.

# Westerly Wind Events in the Eastern Indian Ocean as a Precursor to El Niño: A Case Study for the 2002-03 El Niño

Scott Curtis, Robert F. Adler, George J. Huffman, and Guojun Gu

Submitted Journal of Climate June 20 2003

Abstract:

This study expands on recent work linking intraseasonal to seasonal observed precipitation variability from September to March in the eastern Indian Ocean with the initiation of El Niño events during the last 20 years, by examining locally the strength of daily zonal wind. Westerly winds prevail over the eastern equatorial Indian Ocean year-round. However, southward from the Equator there is a rapid transition from a westerly to an easterly wind regime. A daily climatology of zonal wind averaged over the area 5° to 15°S and 70° to 100°E shows strong easterlies at the beginning and end of the austral summer season, with weak zonal winds in January and February. Days with westerly wind speeds in excess of 1.5 standard deviations were defined as westerly wind burst (WWB) events. A general increase in WWB days is shown during September to March before the onset of El Niños. Finally, this study examines climate variations in the Indo-Pacific sector for the austral summer prior to the 2002-03 El Niño, because January-February-March 2002 contained the largest number of WWB event days in the 1979-2002 climatology, and high-quality high-resolution satellite-based data sets of precipitation, wind, and SST are readily available. Twice, maxima in precipitation and zonal winds propagated eastward, first to the north of the Equator and then to the south. For the southern case, warm waters preceded heavy precipitation in the eastern Indian Ocean, which led strong westerly winds. These climate anomalies followed each other through the ocean passage between Indonesia and Australia, suggesting a coupling of convection, wind, and sea surface temperatures on the time scale of days. Furthermore, this coupling may serve as the mechanism that intensifies and propagates atmospheric disturbances from the Indian to western Pacific Ocean. In this way, it is possible that an

active WWB season in the eastern Indian Ocean would provide the stochastic forcing necessary for El Niño initiation.

## 1. Introduction

Intraseasonal variations in circulation and convection in the Indo-Pacific sector have traditionally been used to describe the Madden-Julian Oscillation (MJO) (eg. Madden and Julian 1994, Meehl et al., 1996). However, recently air-sea interactions associated with the MJO have been observed (eg. Shinoda et al. 1998, Woolnough et al. 2000). This coupling may also be present at shorter time and space scales associated with westerly wind bursts (Harrison and Vecchi 2001). High-quality daily values of wind and sea surface temperature (SST) can be obtained from buoys over the Pacific (TRITON/TAO). This data is routinely assimilated into climate models, which can be used to construct reliable climatologies of subseasonal variability since the mid-1980s (Harrison and Vecchi 1997). However, over most of the tropical oceans this record of data is not yet in existence. Global satellite data at an appropriate temporal and spatial resolution are available during the past several years. The Global Precipitation Climatology Project's (GPCP) one degree daily (1DD) data set (Huffman et al. 2001) is a homogeneous and continuous record of precipitation for the globe since late 1996. The Tropical Rainfall Measuring Mission (TRMM) has provided the highest-quality and highest-resolution precipitation and SST estimates from space since 1998. Scatterometer measurements aboard QuikSCAT also yield globally gridded fields of sea surface wind vectors since 1999. These products allow for detailed case studies of daily climate variations in the tropical oceans and atmosphere over entire seasons leading to new

insights into westerly wind bursts and the MJO. For example, Harrison and Vecchi (2001), using TRMM SST data, examined a rapid cooling in the tropical Indian Ocean during January 1999. The observed cooling was preceded by strong westerly winds south of the Equator.

## 2. Background

The primary motivation for studying the eastern Indian Ocean is our previous work linking intraseasonal oscillations of precipitation in this region with the onset of El Niño since 1979 (Curtis et al. 2002). In summary, it was found that when the dominant climate mode is a gradient of precipitation anomalies across the Equator and strong westerly wind anomalies centered around 95°E in the southern Hemisphere (Fig. 1); and an index of the gradient of precipitation has a pronounced 30-60 day oscillation, then El Niños follow six to nine months later.

This technique was modified to develop a prediction index (PI) based solely on GPCP pentad precipitation data (Xie et al. 2003). Using the time series of the gradient of precipitation anomalies in the eastern Indian Ocean (east box minus west box, Fig. 1), significant ($\geq$ 93%) power in the 30-60 day band of a wavelet analysis and positive trailing six-month mean define a positive El Niño onset prediction (Curtis and Adler 2002). During the development period (1979 to 1999) all but one El Niño was preceded by a positive onset forecast (Fig. 2). The peaks occurred in October, January, and March (Fig. 2). Frequent updates of the PI began in 2001, and in early February 2002 it was found that the January 21-25 2002 value met the necessary conditions for an onset

forecast. In fact, the austral summer season of 2001-02 contains the largest PI values in the record (Fig. 2).

The physical basis for this statistical connection remains unclear. We hypothesize that an active MJO in the eastern Indian Ocean combined with a preconditioned rainfall pattern, consistent with strong westerly winds (Fig. 1), is indicative of convection propagating into the western Pacific, where wind-sea interactions appear to be important for ENSO development. Fig. 3 shows the first eigenvector of a complex principal component analysis of GPCP pentad precipitation anomalies for 1979-2001. The largest variance in the subseasonal precipitation occurs on either side of the Maritime Continent, but the variance in the eastern Indian Ocean leads and is approximately in quadrature to the variance in the western Pacific.

The strength of the 30-60 day variability in zonal wind in the eastern Indian Ocean was not found to be a good predictor for El Niño events (Curtis et al. 2002). However, as previous studies indicate (Vecchi and Harrison 2000, Fedorov 2002), wind bursts with appropriate timing may be more important than MJO-type variations of wind. Thus, a climatology of westerly wind burst (WWB) events in the eastern Indian Ocean is examined in the following section.

## 3. Climatologies

Long term climatologies of NCEP/NCAR reanalysis 1000mb zonal wind (Kalnay et al. 1996) and GPCP Version 2 precipitation (Adler et al. 2003) in the Indian Ocean are shown for September, November, January, and March (Fig. 4), encompassing the Australian monsoon season and periods of positive PI predictions (Fig. 2). Precipitation

associated with the Indian Ocean Convergence Zone is consistently found south of the Equator and is most intense in January (Fig. 4c). Westerly winds in the northern Indian Ocean in September (Fig. 4a) move southward until January (Fig. 4c). For the austral summer season the strongest gradient of zonal wind occurs between 5° and 15° S, suggesting a favored area of vorticity and storm generation (see boxes). We suggest that WWB events are connected to storms and precipitation in the eastern Indian Ocean in a similar manner as in the western Pacific (eg. Harrison and Vecchi 1997, Yu and Rienecker 1998). In the Southern Hemisphere strong westerly winds could be generated on the northern flank of tropical cyclones or to the west of convective complexes. This area is also the entry point for the North Australian Basin, where air-sea coupled MJOs can continue to propagate eastward, unobstructed by the Maritime Continent.

First, monthly climatologies (1979 to 2002) of WWB event days were computed for the box in Figure 4 (5° - 15° S; 70° - 100°E). A WWB event day was defined as a day when the NCEP 1000mb zonal wind was greater than +1.5 standard deviations from the mean, which accounts for less than 8% of the total number of days. The numbers of event days for September-October-November from 1979 to 2001 and Janaury-February-March from 1980 to 2002 are presented in Figure 5.

In general, large numbers of WWB event days occurred during periods of high PI values (Fig. 2). The October 8-12 1981 peak in PI (Fig. 2) corresponded to 16 days of WWBs from September to November 1981 (Fig. 5a). Likewise, the March 7-11 1990 peak in PI (Fig. 2) corresponded to 16 days of WWBs from January to March 1990, with 10 of those days occurring in March (Fig. 5b). Overall the 1996-97 season contained the largest number of WWB event days, with the bulk (23) occurring from September to

November (Fig. 5a). The corresponding peak in the PI occurred on October 18-22 (Fig. 2). Finally, the largest number of WWB event days from January to March occurred during 2002 (Fig. 5b). Every pentad during these months had strong and significant PI values (Fig. 2). Besides the large sample of WWB days in 2001-02, this season serves as a good case study in two respects: 1) high resolution satellite estimates of precipitation, wind, and SST are readily available, and 2) the WWB activity may be related to the largest PI values recorded and subsequent initiation of the 2002-03 El Niño (Curtis et al. 2002).

## 4. Case study

The intraseasonal climate variations from November 2001 to April 2002 were examined using the one degree daily (1DD) precipitation data (Huffman et al. 1999), QuikSCAT wind data, and TRMM microwave imager SST data. 0.25 degree daily resolution wind and SST were obtained from F. Wentz at Remote Sensing Systems (RSS). Only the u-component of wind was used for this study. All data sets were subjected to a 3-day smoother.

Figure 6 shows daily time series of zonal wind, precipitation, and SST averaged over the box in Figure 4 for 2001-02 and climatology. The daily wind climatology (thick lines in Fig. 6a) was constructed from NCEP 1000mb daily zonal winds from 1979 to 2001. Consistent with Fig. 4, the start of November is characterized by strong easterly winds (6 m $s^{-1}$) which weaken until becoming westerly for a few days in February. The winds then become easterly again, reaching speeds of 5 m $s^{-1}$ by the end of April.

Daily estimates of wind from satellites (dashed lines in Fig. 6a) are compared to those from NCEP (solid lines in Fig. 6a), which were used to construct the WWB climatologies. The data sets correlate at 0.98. This is encouraging since the scatterometer data is not assimilated into the NCEP/NCAR model. A WWB occurred in November-December 2001 and again in January-February 2002. The daily precipitation climatology (thick lines in Fig. 6b) is an interpolation of the 1979-98 GPCP Version 2 monthly climatology. The 1DD and Version 2 data sets are consistent in that the 1DD was constructed to add up to the monthly GPCP value (Huffman et al. 2001). Unlike the wind climatology, it shows a weak seasonal cycle with slightly more rain in January-February than in November-December and March-April. The SST climatology (thick line in Fig. 6c), plotted every five days, is a blend of ship observations and satellites (Reynolds and Smith 1994). This independent climatology is meant to show the trending towards higher values during this part of the annual cycle.

Interestingly, in December-January the ocean surface was warmer than normal, followed by copious precipitation, which led a WWB event (Fig. 6). From November 2001 to April 2002 the correlation between 1DD precipitation and QuikSCAT wind reached a maximum of 0.71 when the rainfall led by 9 days. This is consistent with our hypothesis that storms often generate the strong westerly winds. Over that same time period the SST-precipitation correlation was 0.57 when SST led precipitation by 27 days. This suggests a coupling with the surface ocean. Both of these correlations are significant at the 99% level.

Next we examine the climate system of the Indo-Pacific during the November 2001 to April 2002 time period. Particular attention is focused on why the WWB events

and associated climate anomalies occurred in the eastern Indian Ocean (Fig. 6), and if and how they are communicated to the western Pacific (as is suggested by Figs. 2 and 3). Figure 7 shows variable time-longitude diagrams of zonal wind, precipitation, and SST. A running 10 degree latitude average was computed from 20°S to 15°N for each variable every day. The maximum value is plotted as a function of longitude in Fig.7, to show the strongest signal within the deep tropics. The two longest periods of WWB days (Fig. 6a) are depicted as boxes in the left panel. Two eastward propagating wind-rain systems occur in November-December and January-February (Fig. 7, left panel). In the first event the wind (precipitation) travels approximately 2°(2.5°) longitude per day. The actual speeds of the variables are likely faster because this analysis allows for north-south propagation, as well. The rain outpaces the wind, reaching the date line about 11 days earlier. Interestingly, the propagating system appears to be east of 100°E at the time of the WWB event. This relationship will be explored further below.

In the second event, as in the first event, the winds travel eastward at 2° longitude per day. However, the rainfall is slower for this event, leading the winds by 8 days at 60°E, but only by 2.5 days at 180°. The fact that the former lag time is consistent with the lag time between the maximum rainfall and the January-February WWB (Fig. 6), and the system moves through the WWB box (Fig. 7) indicates a more direct relationship between the two, than in the first event. The SST data shows quite strikingly a warming between 60° and 80°E that lasted a few days in early January (Fig. 7, right panel). The warming seems to have initiated, after some lag time, the precipitation-wind event that traveled to the western Pacific. The waters also warmed ahead of the precipitation from 120°E to 180° (Fig. 7, right panel).

In order to examine the track of the two propagating events, the latitude and longitude of the maximum precipitation and wind value in Figure 7 (left panel) was recorded each day. The eastward propagation was confirmed and representative days were selected and plotted in Figure 8. For the first event (Fig. 8a) strong westerly winds were generated just north of the Equator on November 13 and heavy rains began within the area used to define WWBs (see box) on November 15. The wind maximum moved south into the study area and the precipitation and wind were nearly collocated from November 20 to 26. This is consistent with Fig. 7, which shows the wind and rain moving eastward at approximately the same speed in the middle of November. The rainfall maximum moves quickly to the Philippines and the wind traverses just north of the Equator in early December. By December 10 they are nearly collocated once more in the western Pacific. The wind signal is farthest west on December 13, while the precipitation signal continues to travel southeastward and into the vicinity of the South Pacific Convergence Zone on December 23.

Strong winds associated with the second event begin off the coast of Madagascar (Fig. 8b). The rain followed by the wind pass directly through the area used to define the WWBs (see box) in late January. By February 5 the maxima enter the North Australian basin. The strongest winds remain in the Timor Strait for the first half of February, while the rainfall reaches the Pacific Ocean by February 9, and ends its march eastward in the middle of February. The wind maximum moves northward to the coast of New Guinea on February 14, and reaches the equatorial west Pacific on February 25. While the two events would be considered equatorial, they clearly take different tracks from the Indian to the Pacific Oceans, with the first to the north and the second to the south of the

Equator, via the Timor Strait. It could be argued that the second event was more tightly coupled in time and space. Also, the fact that this event tracked almost entirely over ocean may explain the apparently strong coupling with SST in Fig. 7, right panel.

While Figs. 6-8 give an encapsulated summary of WWBs and intraseasonal features of the 2001-02 season, selected maps of precipitation, zonal wind, and SST are presented for completeness. Fig. 9 shows the state of the Indo-Pacific for November 27 and 30 and December 3 and 6. The succession of maps is consistent with the locations of rainfall and wind maxima during these days (Fig. 8a). On November 27 the strongest winds are on the Equator in the eastern Indian Ocean, while the heaviest rainfall is further south over the study area. The bulk of the enhanced westerly winds and rainfall move to the north (as in Fig. 8a). However, there is a center of precipitation, likely associated with a tropical cyclone, that travels to the south (Fig. 9). Thus, strong westerly winds on the north side of the cyclone pass through the study area (Fig. 9b,c,d) resulting in a 9-day WWB event (Fig. 6).

The second WWB event in January-February (Fig. 6) coincides with eastward propagation of strong wind and heavy precipitation (Fig. 7, 8). However, prior to any organization in winds and rainfall (Fig. 10a), high sea surface temperatures are found in a band across the Indian Ocean on June 5 (Fig. 10b). Voids in the SST estimates occur when TMI detects precipitation. These areas are generally located within the largest 1DD precipitation contours. As precipitation builds in the central Indian Ocean (Fig. 10c), the basin cools (Fig. 10d). On January 19, strong westerly winds and heavy precipitation stretch from Sumatra to Madagascar (Fig. 10e, see Fig. 8b), while SSTs increase between Indonesia and Australia (Fig. 10f). On January 26, two centers of rainfall are located to

the west of Sumatra and in the southern Indian Ocean (Fig. 10g). This combination brings strong westerly winds into the study area. The heaviest rainfall is to the north of the winds, consistent with Fig. 8b. The wind-precipitation system moves swiftly eastward over the warmer waters on February 2 (Fig. 11c), leaving cooler waters in its wake (Fig. 11d). At this time the warmest surface waters are found to the east of the rainfall and winds in the Coral Sea (Fig. 11d). On February 9 the precipitation and westerly winds push across the north coast of Australia, while another southern hemisphere cyclone contributes to strong westerly winds over the study region (Fig. 11e). SSTs increase over the western equatorial Pacific and decrease over the North Australian basin (Fig. 11f). On February 16 the propagating system reaches the western Pacific, while wind speeds diminish over the eastern Indian Ocean (Fig. 11g). This sequence of maps (Fig. 11) indicates a strong coupling of precipitation, winds, and SST.

## 5. Discussion

While westerly wind burst (WWB) climatologies have been compiled for the western Pacific, this paper extends the previous work to include the eastern Indian Ocean. The focus of the study was the area: 5° S to 15° S and 70° E to 100° E, where strong westerly wind anomalies are tied to El Niño-related precipitation variability, especially from September to March. WWB days were defined for the study area, and counted for the September-October-November and January-February-March seasons from 1979 to 2002. A large interannual variability was noted, with peaks before El Niño events.

Satellite observations of wind and other climate variables allowed for a detailed case study of the summer of 2001-02. Two distinct periods of strong westerly winds

were observed in the study area. The first was produced by a Southern Hemisphere cyclone after the passage of organized convection to the north of the Maritime Continent. The second was a direct result of organized convection passing to the south of the Maritime Continent and through the Timor Strait. Whether these tracks are typical is open to question. However, we speculate that the convection is coupled with the ocean surface and is steered by the warmest waters during the annual cycle. Thus, a track on the Equator may be less favorable, due to the large islands of Sumatra and Borneo. Of the two propagating systems, the second is more convincingly coupled with the SST. Beginning in January 2002, heavy rains led strong westerly winds by 9 days in the eastern Indian Ocean. The wind-rain system moved over the waters between Indonesia and Australia and into the western Pacific about three weeks later (from approximately January 26 to February 16). Warm waters in the eastern Indian Ocean appeared about a month before the heaviest precipitation, but were not well correlated with the westerly winds. Thus, the warming does not induce WWBs directly, but through the generation of convection. The warm waters continued to lead rainfall to the north of Australia, and into the Pacific.

Finally, the relationship between WWB events in the Indian and Pacific Oceans deserves more attention than can be given in this paper. However the case presented here with high-resolution satellite data is intriguing considering our work linking precipitation and westerly winds in the Indian Ocean to El Niño initiation. Zonal wind stress in the western Pacific, with appropriate *interannual* to *intraseasonal* frequencies, can directly affect El Niño. We have shown that, first, Indian Ocean WWB days are frequent during the austral summers prior to recent El Niño events, and, second, strong westerly winds in

the western Pacific can be traced back to the eastern Indian Ocean. This is consistent with a complex principal component analysis of precipitation anomalies in the Indo-Pacific sector, which shows variations in the eastern Indian Ocean leading variations in the western Pacific. It is proposed that air-sea coupling acts as a bridging mechanism between the two basins by intensifying and propagating atmospheric disturbances from the Indian to Pacific Ocean. In this way, it is possible that an active WWB season in the eastern Indian Ocean provides the stochastic forcing necessary for El Niño initiation.

Acknowledgments: The authors would like to thank Remote Sensing Systems who produced the TMI SST data, sponsored by NASA's Earth Science Information Partnerships (ESIP): a federation of information sites for Earth Science; and by NASA's TRMM Science Team, and QuikScat data, sponsored by the NASA Ocean Vector Winds Science Team. The authors would like to thank Dr. Alberto Mestas Nunez and Dr. David Enfield for supplying the Complex Principal Component Analysis code and for their help in interpreting the results.

Figure Captions

Figure 1. A reproduction of Figure 1b from Curtis et al. (2002). The second combined EOF of precipitation, 1000mb zonal wind, and 1000mb meridional wind anomalies in the Indian Ocean sector. The precipitation is shaded and the zonal wind in contours. Boxes indicate areas used to define the pronounced gradient in precipitation anomalies.

Figure 2. An El Niño onset prediction index (PI) based on the Curtis et al. (2002) study, namely the 30-60 day power of a wavelet analysis of the gradient of precipitation anomalies (see Fig. 1). Black (gray) bars indicate pentads that have a positive (negative) trailing six-month mean. Only black bars are considered, and arrows indicate pentads of PI maxima in excess of the 93% significance level (dashed line).

Figure 3. First eigenvector from a complex principal component analysis of GPCP pentad precipitation from 1979 to 2001 (explains 11.74% of the variance). A vector is plotted at each grid box so that its length is proportional to its magnitude and its angle is proportional to its relative phase. Propagation occurs in the direction of counterclockwise rotation. Contours denote the 0.2 and 0.3 levels of local variance explained.

Figure 4. Climatologies of 1000mb zonal wind (contours) and precipitation (shading). Contours are every 2 m $s^{-1}$. Box (5°S - 15°S; 70°E - 100°E) indicates area used to define westerly wind burst events. a) September, b) November, c) January, d) March

Figure 5. Number of westerly wind burst (WWB) days over the box shown in Figure 4 for a) September-October-November 1979 to 2001 and b) January-February-March 1980 to 2002. Data is daily NCEP/NCAR reanalysis 1000mb zonal wind anomalies. A WWB day is defined as having a wind value greater than +1.5 standard deviations.

Figure 6. November 2001 to April 2002 time series of daily zonal wind, precipitation, and SST values averaged over the box shown in Figure 1. a) NCEP/NCAR 1000mb zonal wind (thin solid line), zonal wind climatology (thick solid line), and QuikSCAT sea surface zonal wind (thin dashed line). b) precipitation (thin solid line) and precipitation climatology (thick solid line). c) SST (thin solid line) and pentad SST climatology (thick solid line). Dots in a) indicate westerly wind burst days (see Figure 5).

Figure 7. Variable time-longitude diagrams of zonal wind, rainfall, and SST for 40°E to 160°W and from November 2001 to April 2002. The maximum value of a running 10 degree latitude average from 20°S to 15°N is plotted for each variable. Left panel is QuikSCAT overlain with contours of 1DD precipitation (15, 20, 25, 30, 35, 40, and 45 mm $day^{-1}$). Right panel is SST from TRMM overlain with contours of 1DD precipitation (15, 20, 25, 30, 35, 40, and 45 mm $day^{-1}$).

Figure 8. Lines connect the locations of the maximum values of zonal wind and precipitation in Fig. 7 (left panel) for selected days. Dashed line and closed circles are

for precipitation, and solid lines and open circles for wind. . Box (5°S - 15°S; 70°E - 100°E) indicates area used to define westerly wind burst events.

Figure 9. Three-day averages of zonal wind from QuikSCAT overlain with contours of 1DD precipitation (10, 20, and 30 mm $day^{-1}$) for a period in late November and early December 2001.

Figure 10. Three-day averages of zonal wind from QuikSCAT (left) and SST from TRMM (right) overlain with contours of 1DD precipitation (10, 20, and 30 mm $day^{-1}$) for a period in January 2002.

Figure 11. A continuation of Figure 10 into February 2002.

References

Adler, R. F., G. J. Huffman, A. Chang, R. Ferraro, P. Xie, J. Janowiak, B. Rudolf, U. Schneider, S. Curtis, D. Bolvin, A. Gruber, J. Susskind, and P. Arkin, 2003: The Version 2 Global Precipitation Climatology Project (GPCP) monthly precipitation analysis (1979-present). *J. Hydrometeor.*, in press.

Curtis, S., and R. F. Adler, 2002: GPCP precipitation anomalies in the Indian Ocean as precursors to El Niño. *GEWEX News*, 12 (1), 10.

Curtis, S., G. J. Huffman, and R. F. Adler, 2002: Precipitation anomalies in the tropical Indian Ocean and their relation to the initiation of El Niño. *Geophys. Res. Lett.*, 29(10), 1441, doi:10.1029/2001GL01339.

Federov, A. V., 2002: The response of the coupled tropical ocean-atmosphere to westerly wind bursts. *Q. J. R. Meteorol. Soc.*, 128, 1-23.

Harrison, D. E., and G. A. Vecchi, 1997: Westerly wind events in the tropical Pacific, 1986-95. *J. Climate*, 10, 3131-3156.

Harrison, D. E., and G. A. Vecchi, 2001: January 1999 Indian Ocean cooling event. *Geophys. Res. Lett.*, 28, 3717-3720.

Huffman, G. J., R. F. Adler, M. Morrissey, D. T. Bolvin, S. Curtis, R. Joyce, B. McGavock, and J. Susskind, 2001: Global precipitation at one-degree daily resolution from multi-satellite observations. *J. Hydrometeor.*, 2, 36-50.

Kalnay, E., M. Kanamitsu, R. Kistler, W. Collins, D. Deaven, L. Gandin, M. Iredell, S. Saha, G. White, J. Janowiak, K. C. Mo, C. Ropelewski, J. Wang, A. Leetmaa, R. Reynolds, R. Jenne, and D. Joseph, 1996: The NCEP/NCAR 40-year reanalysis project. *Bull. Amer. Meteor. Soc.*, 77, 437-471.

Madden, R. A., and P. R. Julian, 1994: Observations of the 40-50 day tropical oscillation–a review. *Mon. Wea. Rev.*, 122, 814-835.

Meehl, G. A., G. N. Kiladis, K. M. Weickmann, M. Wheeler, D. S. Gutzler, and G. P. Compo, 1996: Modulation of equatorial and subseasonal convective episodes by tropical-extratropical interaction in the Indian and Pacific Ocean regions. *J. Geophys. Res.*, 101, 15033-15049.

Reynolds, R. W., and T. M. Smith, 1994: Improved global sea surface temperature analyses using optimum interpolation. *J. Climate*, 7, 929-948.

Shinoda, T., H. H. Hendon, and J. Glick, 1998: Intraseasonal variability of surface fluxes and sea surface temperature in the tropical western Pacific and Indian Oceans. *J. Climate*, 11, 1685-1702.

Vecchi, G. A., and D. E. Harrison, 2000: Tropical Pacific sea surface temperature anomalies, El Nino, and equatorial westerly wind events. *J. Climate*, 13, 1814-1830.

Woolnough, S. J., J. M. Slingo, and B. J. Hoskins, 2000: The relationship between convection and sea surface temperature on intraseasonal timescales. *J. Climate*, 13, 2086-2104.

Xie, P., J. E. Janowiak, P. A. Arkin, R. Adler, A. Gruber, R. Ferraro, G. J. Huffman, and S. Curtis, 2003: GPCP pentad precipitation analyses: An experimental data set based on gauge observations and satellite estimates. *J. Climate*, in press.

Yu, L., and M. M. Rienecker, 1998: Evidence of an extratropical atmospheric influence during the onset of the 1997-98 El Niño. *Geophys. Res. Lett.*, 25, 3537-3540.

Figure 1

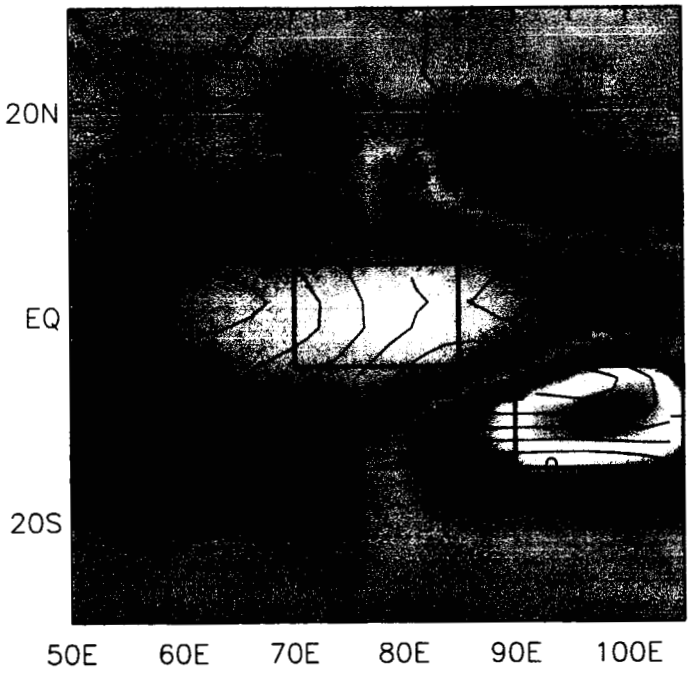

Figure 2

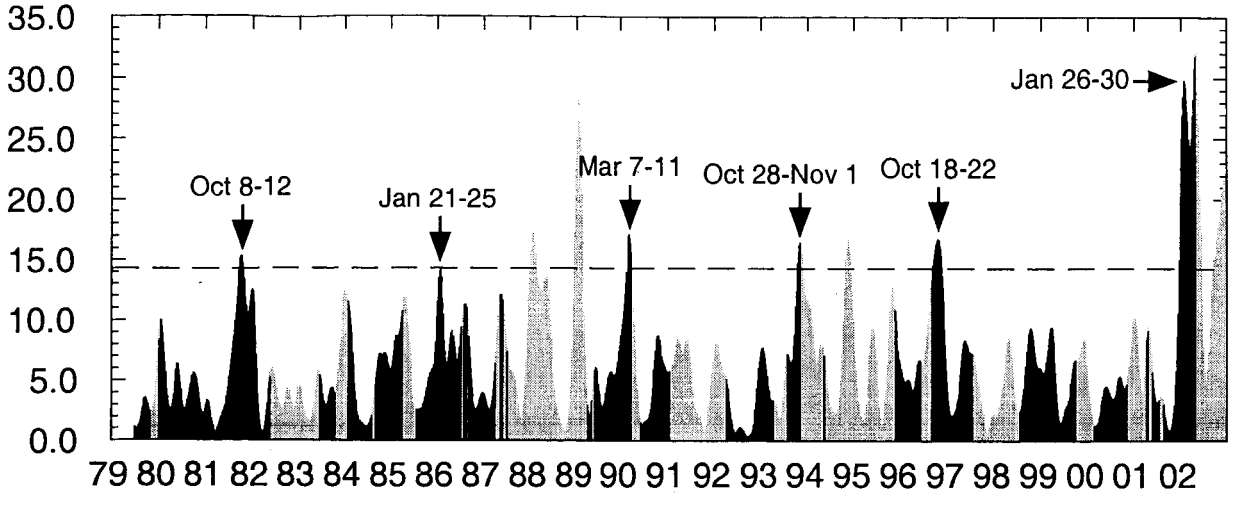
35.0
30.0
25.0
20.0
15.0
10.0
5.0
0.0
Oct 8-12
Jan 21-25
Mar 7-11
Oct 28-Nov 1
Oct 18-22
Jan 26-30
79 80 81 82 83 84 85 86 87 88 89 90 91 92 93 94 95 96 97 98 99 00 01 02

Figure 3

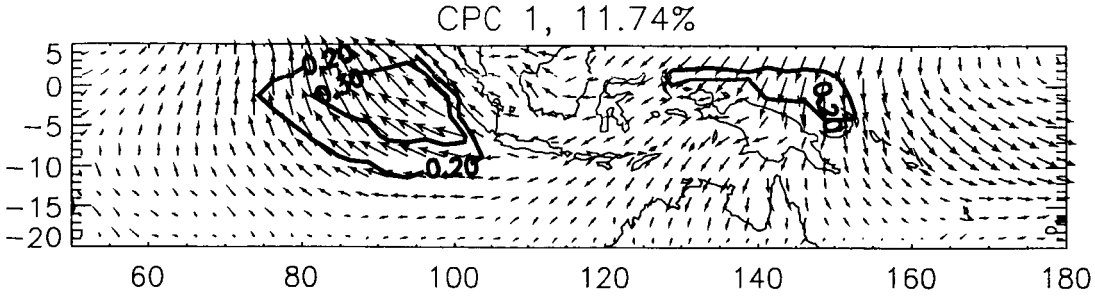

Figure 4

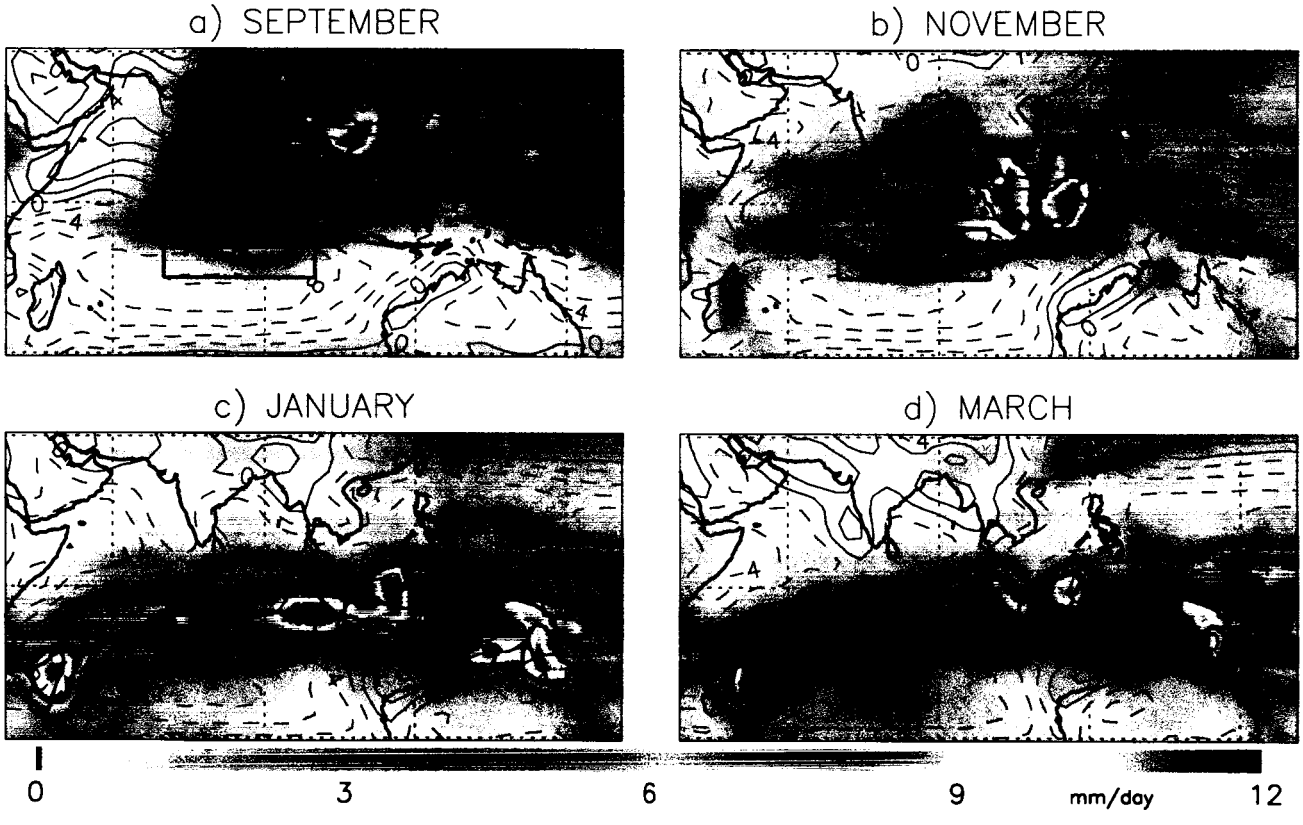

Figure 5

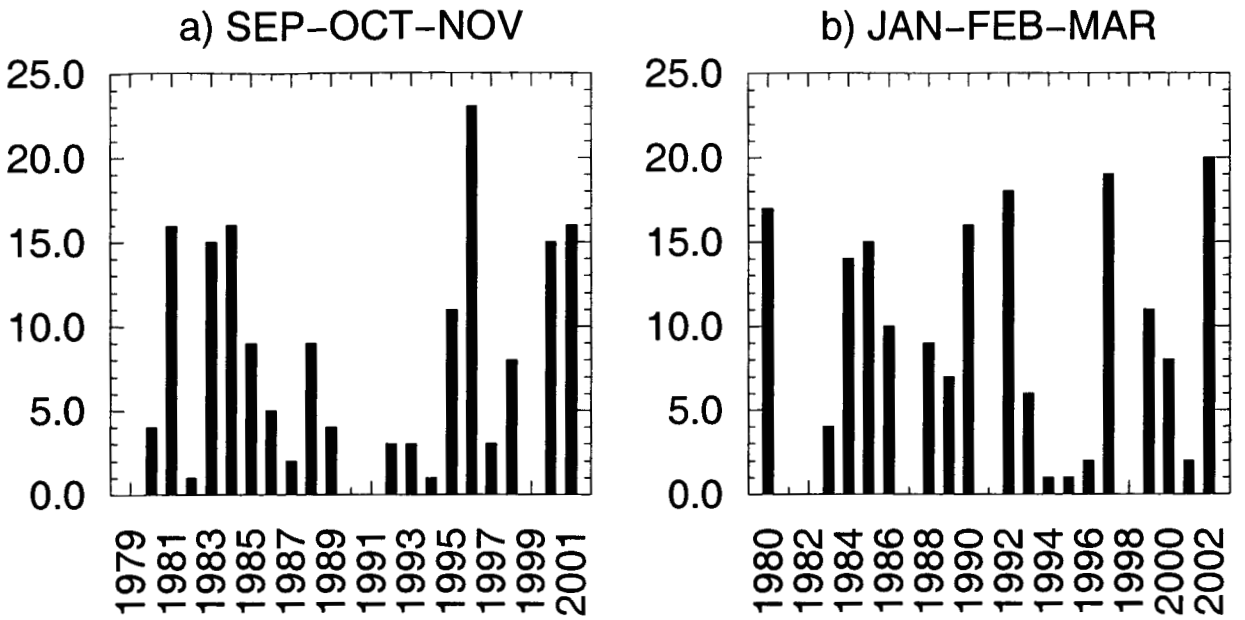
a) SEP–OCT–NOV
25.0
20.0
15.0
10.0
5.0
0.0
1979
1981
1983
1985
1987
1989
1991
1993
1995
1997
1999
2001
b) JAN–FEB–MAR
25.0
20.0
15.0
10.0
5.0
0.0
1980
1982
1984
1986
1988
1990
1992
1994
1996
1998
2000
2002

Figure 6

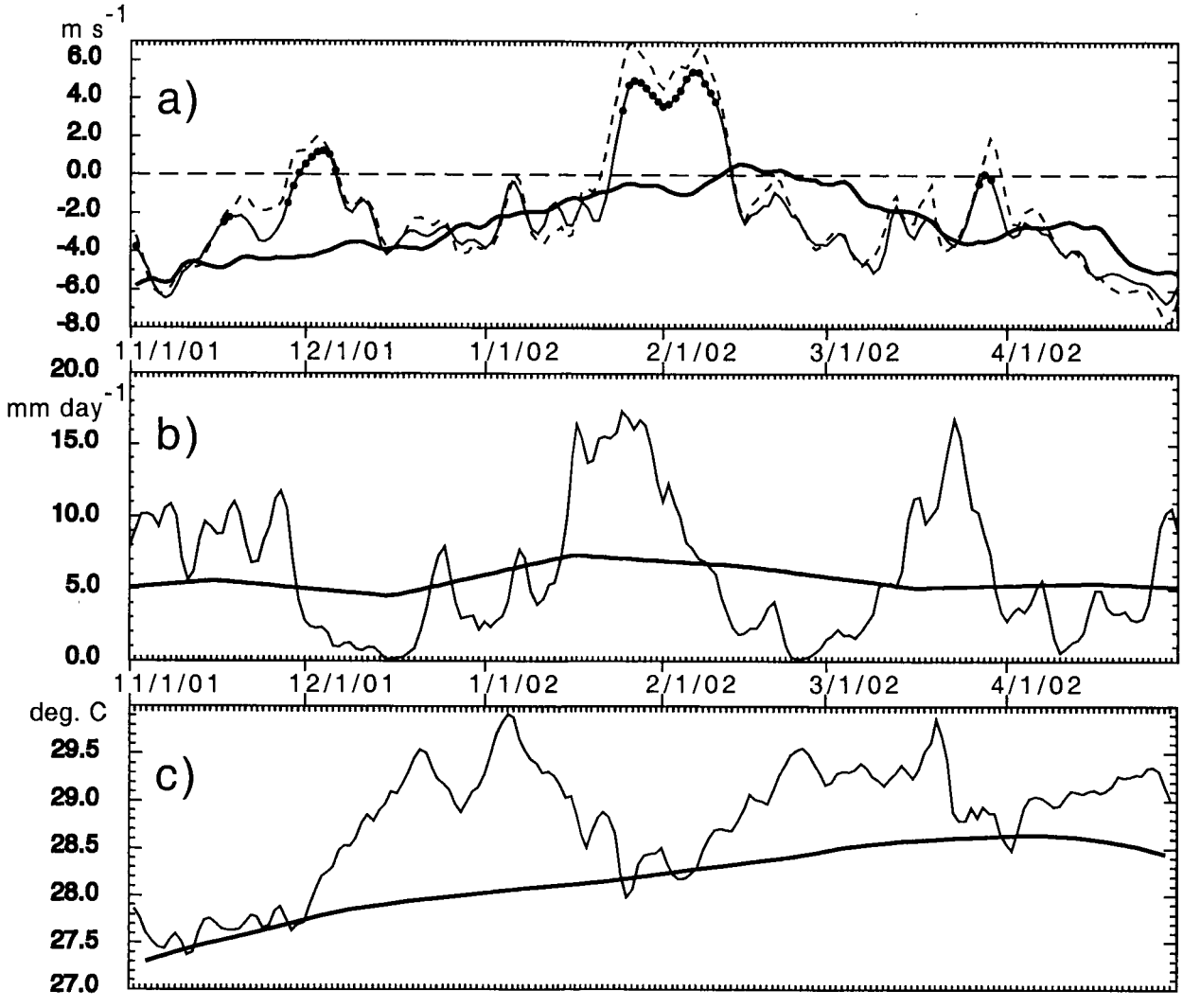
m s-1
6.0
4.0
2.0
0.0
-2.0
-4.0
-6.0
-8.0
a)
11/1/01
12/1/01
1/1/02
2/1/02
3/1/02
4/1/02
20.0
mm day-1
15.0
10.0
5.0
0.0
b)
11/1/01
12/1/01
1/1/02
2/1/02
3/1/02
4/1/02
deg. C
29.5
29.0
28.5
28.0
27.5
27.0
c)

Figure 7

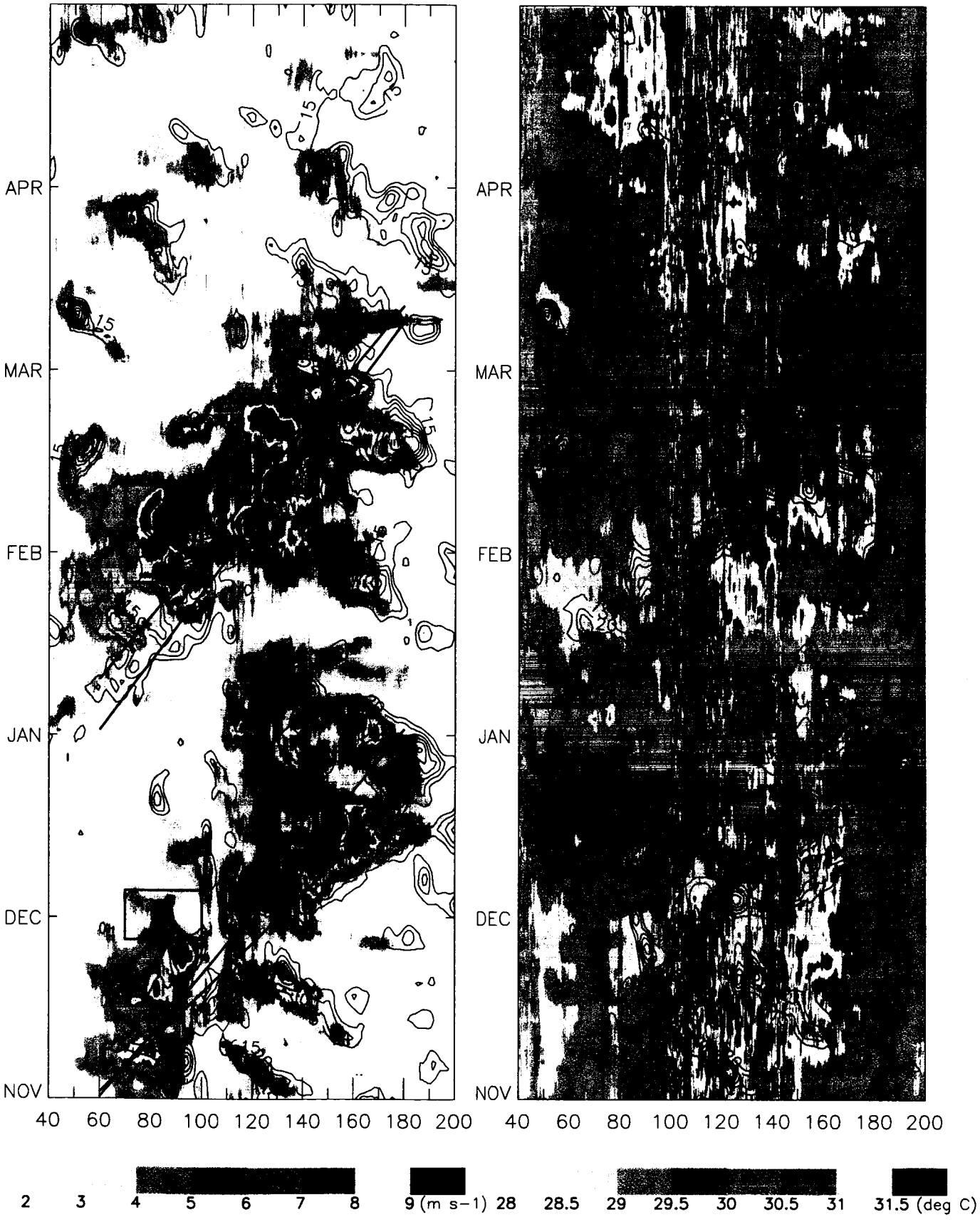
APR
MAR
FEB
JAN
DEC
NOV
40 60 80 100 120 140 160 180 200
APR
MAR
FEB
JAN
DEC
NOV
40 60 80 100 120 140 160 180 200
2 3 4 5 6 7 8 9 (m s−1) 28 28.5 29 29.5 30 30.5 31 31.5 (deg C)

Figure 8

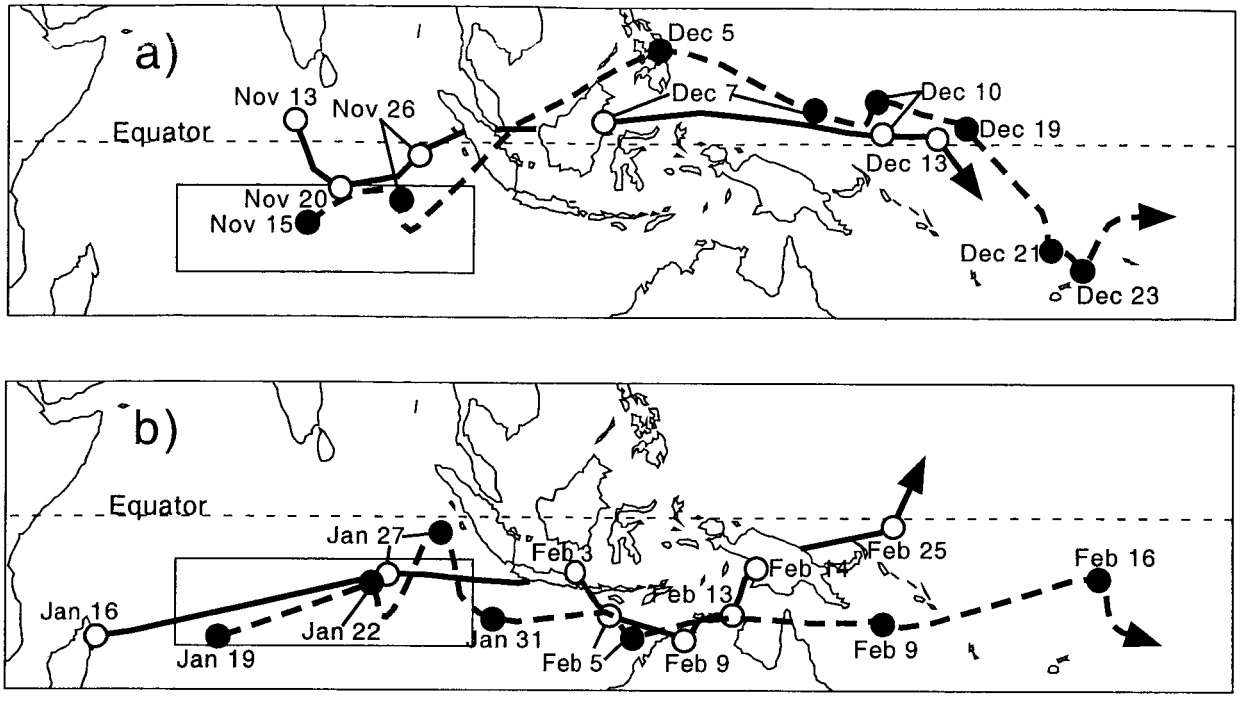
a)
Equator
Nov 13
Nov 26
Nov 20
Nov 15
Dec 5
Dec 7
Dec 10
Dec 19
Dec 13
Dec 21
Dec 23
b)
Equator
Jan 16
Jan 19
Jan 22
Jan 27
Jan 31
Feb 3
Feb 5
Feb 9
Feb 13
Feb 14
Feb 25
Feb 9
Feb 16

Figure 9

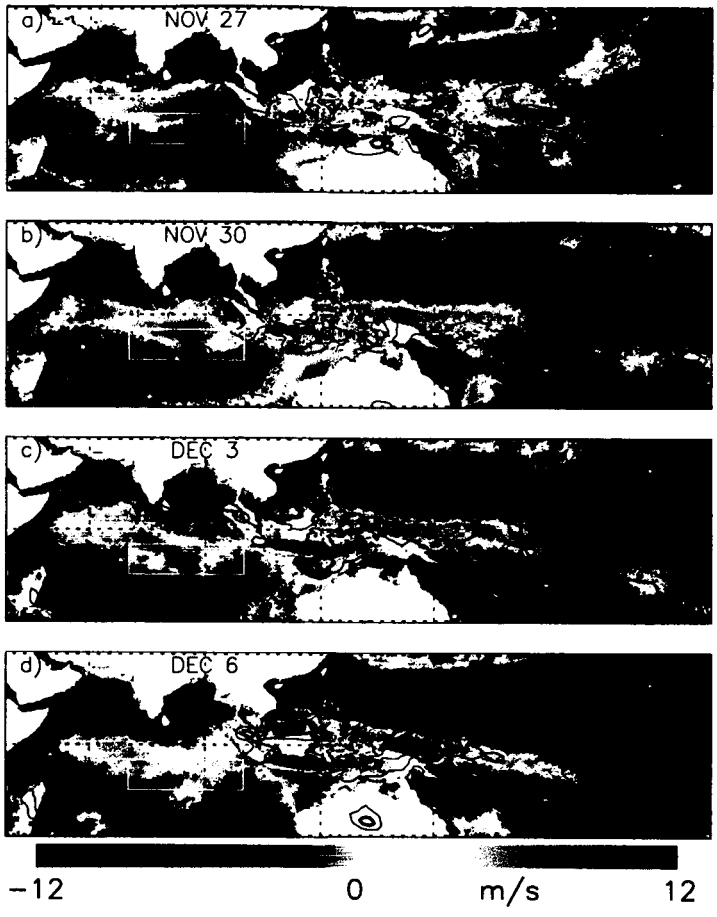

Figure 10

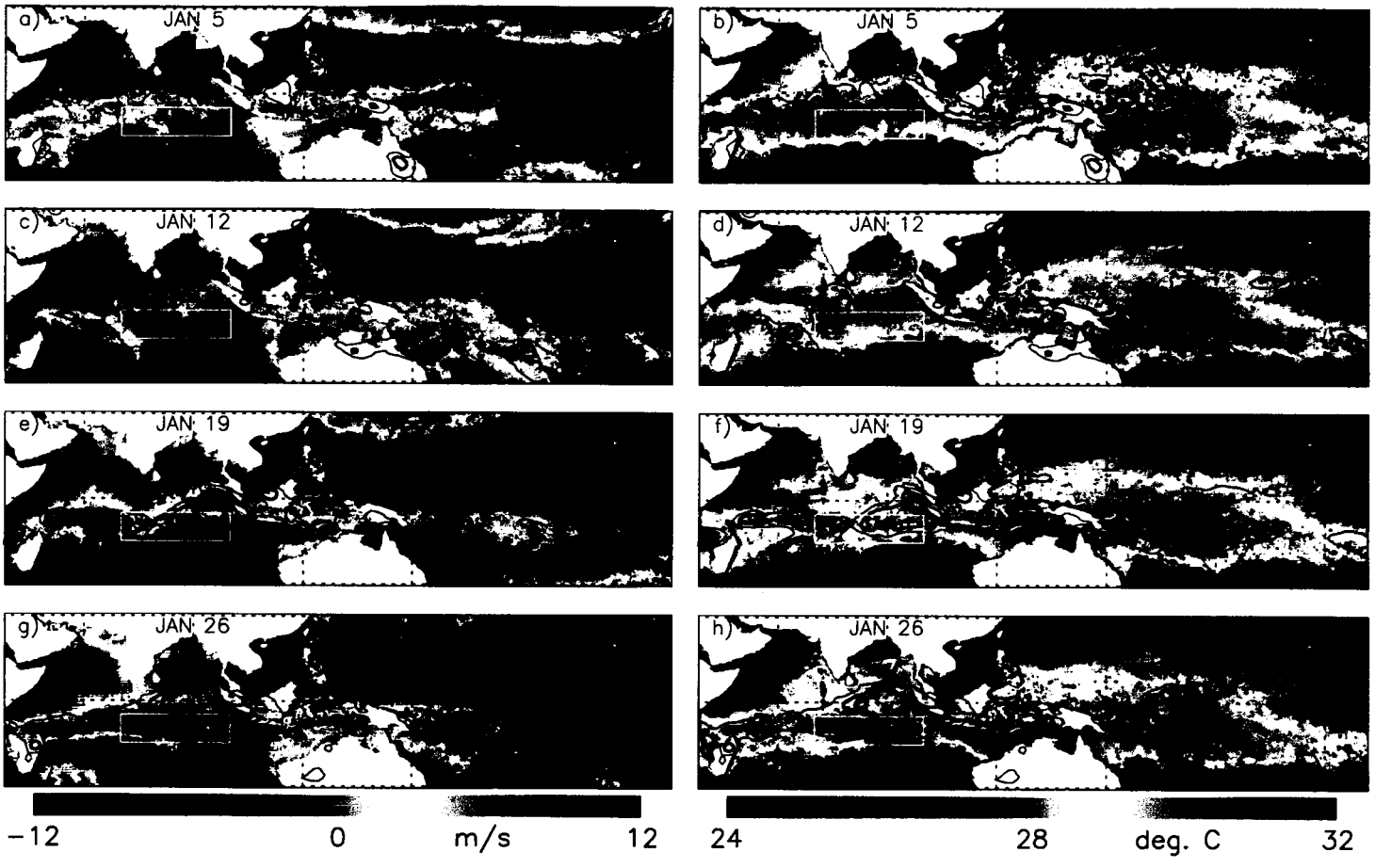
a) JAN 5
b) JAN 5
c) JAN 12
d) JAN 12
e) JAN 19
f) JAN 19
g) JAN 26
h) JAN 26
−12
0
m/s
12
24
28
deg. C
32

Figure 11

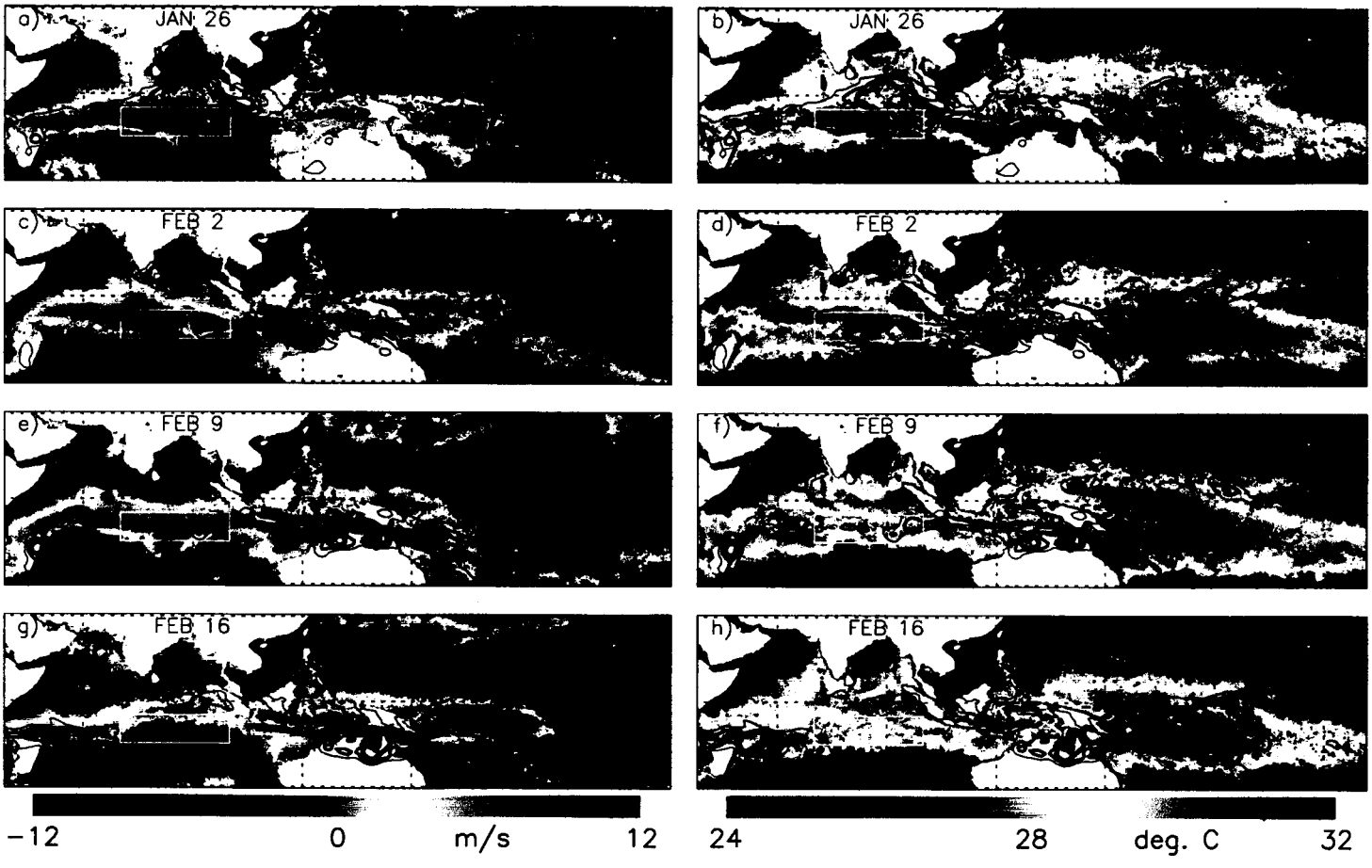
a) JAN 26
b) JAN 26
c) FEB 2
d) FEB 2
e) FEB 9
f) FEB 9
g) FEB 16
h) FEB 16
−12
0
m/s
12
24
28
deg. C
32